Journal of Materials Chemistry A

Accepted Manuscript

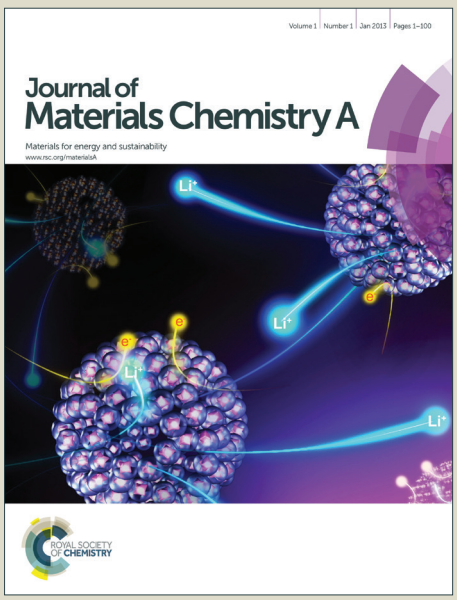

ROYAL SOCIETY OF CHEMISTRY

www.rsc.org/materialsA

Journal of Materials Chemistry A RSCPublishing

ARTICLE

ZIF-8 micromembranes for gas separation prepared on laser-perforated brass supports

Cite this: DOI: 10.1039/xoxxoooooox

Marta Navarro,[a,b] Beatriz Seoane,[a] Ester Mateo,[c] Ruth Lahoz,[d] Germán F. de la Fuente[d] and Joaquín Coronas[a,*]

Received ooth January 2012,
Accepted ooth January 2012

DOI: 10.1039/xoxxoooooox

www.rsc.org/

ZIF-8 is an imidazolate-based metal-organic framework (MOF). ZIF-8 micromembranes of 20-32 μm in diameter are prepared by synthesizing the MOF on Nd-YAG laser-perforated 75 μm thick brass sheets (63/37 Cu/Zn). The laser irradiation activates the brass support, promoting ZIF-8 growth. A thick and continuous ZIF-8 membrane is crystallized on the laser irradiation outlet side of the support, while the inlet side and the inner surface of the microperforations are also coated with ZIF-8 intergrowth crystals. Laser perforated brass supports are not only cheap, flexible, strong, easy to handle and to process as membrane materials; they are also chemically compatible with the ZIF-8 composition because of the shared Zn element. The ZIF-8 membranes obtained are characterized by XRD, SEM, TGA and N_2 sorption analysis. Furthermore, the membranes are applied to the separation of equimolar H_2/CH_4, He/CH_4, CO_2/CH_4 and O_2/N_2 mixtures confirming the expected molecular sieving effect due to MOF microporosity.

Introduction

Metal-organic frameworks (MOFs) are porous solids obtained from the reaction between organic and inorganic species. The corresponding anionic organic moieties, mostly carboxylate, phosphonate, sulfonate or imidazolate ions, act as a bridge between the metal centers to yield open, crystalline, porous structures.[1,2] Due to their high pore volume and specific surface area values,[3] flexibility,[4] and ease of modifying functionalities in the pores,[5,6] these materials have applications in the fields of adsorption,[7] encapsulation,[8] drug delivery,[9] separation and storage of gases and vapors,[10,11] catalysis,[12] sensors[13] and membranes.[14]

Compared to other separation operations, membrane technology is more efficient considering both energy cost and separation selectivity. This is why the study of zeolite and MOF membranes has intensified considerably during the last few years.[14-17] However, there is still a long way to go before this type of membrane will be commercially available. A number of barriers must be overcome relating to reproducibility, cost, performance and processability.[14] The only industrial-scale application of zeolite membranes to date is in the dehydration of solvents by pervaporation.[18] It should be noted that commercial applications of zeolite or MOF membranes do not necessarily imply dimensions of many square meters of permeation area in a single unit.[14,19] Scaling-down, e.g. producing micromembranes, should allow the preparation of true defect-free membranes that would have a higher chance of tolerating the chemical and physical stresses produced during the activation and performance stages.

Bottom-up and top-down approaches have been developed for controlling MOF attachment on a given support.[20] Bottom-up approaches include seeding methodologies using metal nanoparticles as MOFs precursors,[21] magnetic manipulation,[22] chemical surface modification,[23] microcontact printing,[24] microfluidics and layer by layer deposition of MOF coatings,[25] galvanic displacement[26] and plasma polymer coating patterning before MOF growth.[27] Top-down methodologies involve different types of photolithography and microcontact printing. They are independent of the porous coating formation and thus allow an easy patterning process.[13, 28]

In this work, the growth of ZIF-8 crystals on a brass metallic support was controlled by laser irradiation of the support previous to MOF liquid phase synthesis. This approach promoted growth on restricted, laser irradiated areas (i.e. lines or microholes). Metallic supports are cheap and easy to handle and process, they can withstand high temperatures and exhibit good flexibility and mechanical strength. In particular, brass is the most widely used copper-based alloy because of its good corrosion resistance, formability, high strength and hot-working properties.[29] Brass is an alloy made of Cu and Zn. The Zn in the support is thus compatible with the MOF to be grown (ZIF-8) with the chemical formula $Zn(MeIM)_2$, where MeIM corresponds to 2-methylimidazolate.[30] ZIF-8 has SOD zeolitic

topology with Zn atoms bonded to imidazolate ligands, resulting in a porous framework with large cavities of 11.6 Å diameter interconnected by small 3.4 Å windows.[30] This pore limiting dimension of 3.4 Å is within the range of the kinetic diameters of several gas molecules of great industrial and environmental concern (e.g. He, H_2, CO_2 and CH_4), suggesting potential for gas separation applications.[31-34] Another significant property is its framework flexibility, caused by a swing effect of the linker which produces an increase in the window size.[35] This effect may hinder the expected sharp molecular sieving which characterizes zeolites,[33,34,36,37] while it may also be responsible for the adsorption/encapsulation of large molecules (e.g. caffeine[8]) which a priori could not diffuse through its structure.

Both composite mixed matrix membranes (MMMs)[38] and continuous membranes based on ZIF-8 and prepared on porous supports have been reported. In fact ZIF-8 has been grown to form membranes in different types of supports such as titania disc,[32] hollow zirconia fiber,[39] macroporous silica,[40] alumina disc[34,36,37,41,42] or tube[32] and carbon nanotube coated polyethersulfone.[43] There are no reports on the use of laser microperforated metal (brass) sheets as a support to produce MOF membranes. The closest precedent to this work dealt with the preparation of silicalite-1 micromembranes on laser perforated stainless steel sheets.[44] In the present work, the metal support composition-MOF ZIF-8 chemical matching seems to be optimum due to the presence of Zn as a shared element in both parts, and this represents an ideal opportunity. Finally, in addition to performing simultaneous separation and reaction operations in the same way as conventional zeolite or MOF membranes, porous micromembranes may provide easy integration into other microsystems and allow better operational (e.g. temperature) control with an easier commercialization in a highly compact format.[19]

Experimental

Laser irradiation of brass supports

Polished brass sheets (63.4/36.6 atomic%, 62.7/37.3 wt% Cu/Zn from Goodfellow) were used, with dimensions of 0.15 mm x 10 mm x 13 mm and 0.075 mm x 24 mm x 24 mm. Previous to the irradiation, the supports were cleaned in an ultrasound bath for 10 min with acetone followed by a further 10 min in methanol, and then dried in an oven at 60 °C. Two different laser irradiation patterns were followed.

First, to study the control of ZIF-8 crystal growth on the irradiated metal surface, thicker 0.15 mm x 10 mm x 13 mm non-perforated brass supports were irradiated following a linear path. This approach allows limiting the MOF growth to the laser activated region of the brass sheet. A 20 W nominal power Nd:YAG laser manufactured by Rofin Sinar Laser GmbH (model PowerLine E20), emitting at a wavelength of 1064 nm in pulsed mode, was used to irradiate the brass supports. The laser beam scanned the surface twice using a surface scan rate of 100 $mm \cdot s^{-1}$, a laser nominal power of 6 W, a pulse repetition rate of 20 kHz and a pulse width of 80 ns. This led to an irradiance of 50 $MW \cdot cm^{-2}$.

Second, areas of 10 mm x 10 mm were perforated by laser irradiation in thinner 0.075 mm x 24 mm x 24 mm brass supports. In this case two types of lasers and operation conditions were used leading to type I and type II supports, which mainly differ in porosity (dimension of the perforations and distance between them). Type I supports were perforated using the laser system (Rofin Sinar) described in the previous paragraph, while type II were perforated using a 20 W Q-witched Nd:YAG fiber laser system from Jenealogia (model EasyMarck-20), diode-pumped, emitting at a wavelength of 1064 nm (Table 1). We will distinguish throughout the paper between the irradiation inlet and outlet sides of the brass support.

Synthesis of ZIF-8

By applying the previously reported in situ method[31] we were able to promote the crystal growth and the membrane formation of ZIF-8 around the microholes created on the surface of the brass support by the laser irradiation treatments.

To prepare the synthesis solution, 0.270 g of zinc chloride (99%, Sigma-Aldrich), 0.243 g of 2-methylimidazole (>99%, Sigma-Aldrich) and 0.135 g of sodium formate (>99%, Sigma-Aldrich) were added to 20 mL of methanol (>99.8%, Scharlau). The mixture was then treated in an ultrasound bath for approximately 5 min until complete dissolution. Simultaneously, a laser irradiated brass support was placed vertically inside a stainless steel Teflon®-lined autoclave using a Teflon® holder. The synthesis gel was then poured into the autoclave and was allowed to age for 20 min at room temperature. Afterwards, the autoclave was sealed, heated at 8 °C min^{-1} to 100 °C and maintained at 100 ºC for 4 h (for non-perforated brass), 7 h (for perforated brass with 1.6 ± 0.2% porosity) and 8 h (for perforated brass with 18 ± 2% porosity). Finally, after cooling, the supports were rinsed with fresh methanol, ultrasonicated in methanol at RT for 2 min and dried overnight at room temperature to evaporate the solvent.

Characterization

The continuity of the ZIF-8 layer over the perforated support was assessed first by inspection using optical microscopy. Phase purity and possible ZIF-8 crystal orientation were examined by X-ray diffraction (XRD) at ambient temperature on a rotating anode diffractometer (D-Max Rigaku), using monochromatic CuKα radiation with λ=1.5418 Å at a scanning rate of $0.03° \cdot s^{-1}$. Both sides of the perforated supports were analyzed by XRD. Size, morphology and intergrowth of the ZIF-8 crystals were checked by scanning electron microscopy (SEM) operating at 5-10 keV (Quanta FEG 250). The microscopy works have been conducted in the Laboratorio de Microscopias Avanzadas at Instituto de Nanociencia de Aragon. Besides, EDX ("Energy-dispersive X-ray spectroscopy") was used to determine the atomic composition of the phases deposited on the support. The complete removal of the solvent from the ZIF-8 crystals in the micromembranes

Journal of Materials Chemistry A RSCPublishing

ARTICLE

Table 1. Nd:YAG lasers emitting at a wavelength of 1064 nm and ablation conditions used to perforate the brass sheet, and the follow-up porosity. Pulse repetition rate and beam diameter were 4 kHz and 20 μm, respectively.

Support	Laser	Pulse width (ns)	Irradiance ($W \cdot cm^{-2}$)	Scan rate ($mm \cdot s^{-1}$)	Perforation diameter (μm)		Porosity (%)
					Inlet	Outlet	
Type I	Rofin Sinar	10	$4.5 \cdot 10^{10}$	1500	72 ± 12	20 ± 2	1.6 ± 0.2
Type II	Jenealogia	100	$2.5 \cdot 10^{9}$	500	59 ± 1	32 ± 2	18 ± 2

before the gas experiments was checked by thermogravimetry, using a Mettler Toledo TGA/DTA 851^e SF/1100 °C thermogravimetric system. Experiments were performed in N_2 atmosphere (10 mL(STP)·min^{-1}) at 850 °C with a heating rate of 10 °C min^{-1}. N_2 adsorption experiments were carried out at 77 K with a TriStar 3000 supplied by Micromeritics, after outgassing the samples at 110 °C for 10 h.

Permeation performance

To adjust the micromembranes to the permeation modulus, they were glued with Araldite® epoxy resin on an aluminum adhesive disk (diameter 4.4 cm) with a hollow circle where the membrane was placed over an area of 0.6-1.0 cm^2 (Figure S1), depending on the sample. The ensemble was placed in a stainless steel membrane module composed of two stainless steel parts with a cavity in which to place the membrane and a macroporous disk support (20 μm nominal pore size, Mott Co.). The module was sealed with Viton o-rings to avoid gas leakages. Mass flowmeter controllers (Alicat Scientific) were used for feed and sweep gas provision to the membrane module. The total pressure was maintained at 1 atm at the feed or retentate side with pressure gradient values across the membrane close to zero (0.9-1.7 and 3.3-4.2 kPa for type I and type II micromembranes, respectively). 25/25 cm^3(STP)·min^{-1} H_2/CH_4, He/CH_4, CO_2/CH_4 or O_2/N_2 mixtures were fed to the retentate membrane side. Ar (5 cm^3(STP)·min^{-1}) was used as sweep gas for H_2/CH_4, He/CH_4 and O_2/N_2 mixtures, while He (5 cm^3(STP)·min^{-1}) for CO_2/CH_4 mixture. Contrapermeation was estimated as 4.1, 0.5, 1.7 and 0.0 % of sweep gas flow for H_2/CH_4, CO_2/CH_4, He/CH_4 and O_2/N_2 mixtures, respectively. For the three mixtures the permeation measurements were performed at 35 °C. To gain insight into the temperature response of the micromembranes, the H_2/CH_4 mixture separation was also studied in the 35-150 °C range. Gas concentrations in the outgoing stream were analyzed by an online Agilent 3000 A gas micro-chromatograph, equipped with TCD. Permeance results, in mol·m^{-2}·s^{-1}·Pa^{-1}, were obtained once the exit stream of the membrane was stabilized. The separation selectivity of the mixtures was calculated as permeance ratios.

Results and discussion

Linear patterns

Linear patterns were irradiated over brass supports as a starting point to understand the role of laser irradiation in the control of the patterning growth of ZIF-8 crystals. The width of the activated surface (rough groove produced by the irradiation) was about 33 μm with a depth of about 16 μm (Figure 1a and 1b).

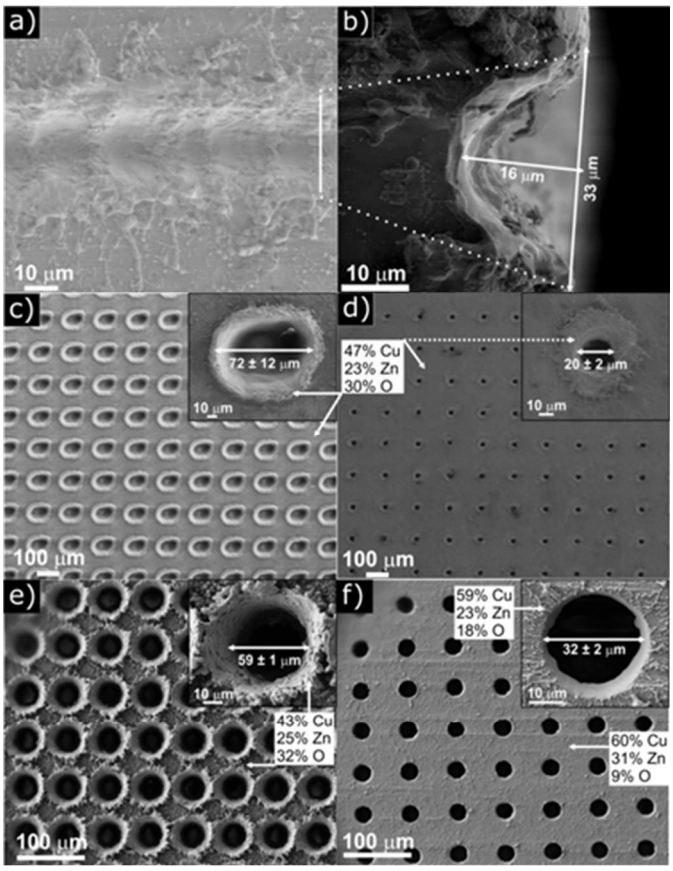

Figure 1. SEM images of: a) laser irradiated brass following a linear path with inset showing fresh support; b) cross section of the rough channel produced upon laser irradiation; c) inlet (rough) and d) outlet (smooth) sides of a type I brass support; e) inlet (rough) and f) outlet (smooth) sides of a type II brass support. EDX atomic compositions are given.

This straight channel clearly promoted the synthesis of ZIF-8, as suggested by the observation of two highly intergrown and twined parallel MOF lines. These were in contrast with the non-irradiated brass surface where intergrowth and twining was considerably lower (Figure 2a and 2b). ZIF-8 heterogeneous nucleation was probably favored by both the roughness created by the laser ablation and the chemical composition of brass rich in Zn (37 wt%), the metal used to build the MOF. The atomic compositions obtained by EDX of different irradiated and non-irradiated bare support areas are shown in Figure 1. As observed, the laser irradiation not only produced the ablation of the metallic support but also its local oxidation, most likely producing ZnO (see Figure S2 where asterisks evidence the presence of the oxide). The latter is more suitable for the MOF synthesis than metallic Zn. In fact, the formation of a ZnO layer on an alumina support in the presence of sodium formate has been reported to promote the heterogeneous nucleation of ZIF-8.[45,46]

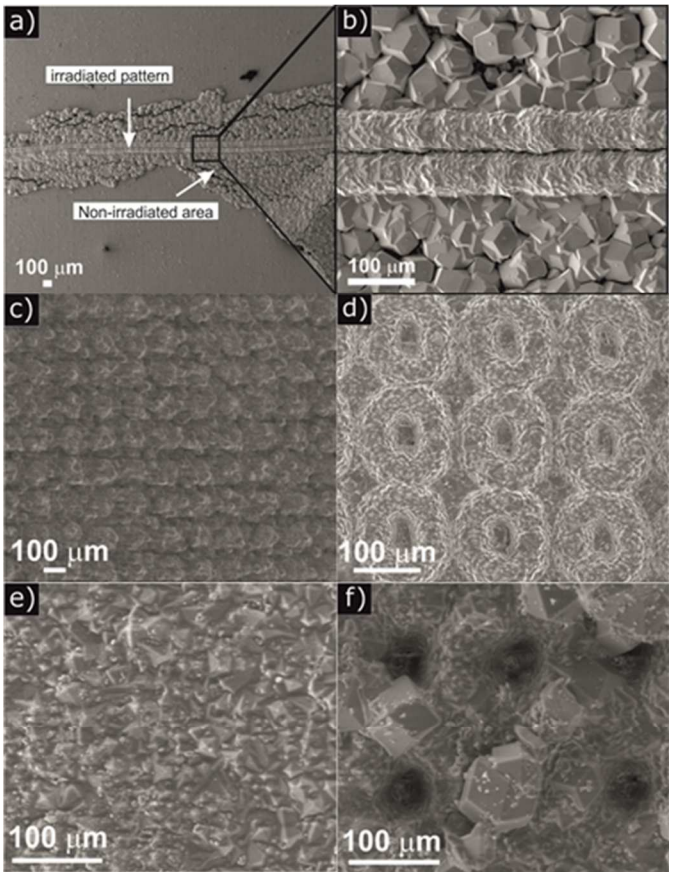

Figure 2. SEM top view images of: a) ZIF-8 growth on linearly irradiated and non-irradiated regions of brass support; b) detail of panel a); c) smooth (irradiation outlet) and d) rough (irradiation inlet) sides of a type I micromembrane; e) smooth (irradiation outlet) and f) rough (irradiation inlet) sides of type II micromembrane.

The fact that the standard reduction potential of Cu (0.337 V) is much higher than that of Zn (-0.763 V) explains the formation of ZnO instead of Cu oxides (Cu2O and CuO). Besides, Cu has a considerably higher boiling point (2562 ºC) than Zn (907 ºC), consistent with the observed increase of the Cu/Zn atomic ratio in the laser affected regions where selective ablation removed Zn at a higher rate than Cu. Loss of the original stoichiometry may thus partially be explained by the fact that a Zn-rich liquid phase appears at the high temperatures reached in the laser irradiated areas.[47] Furthermore, the issue of whether Zn oxidizes while in the liquid phase or in the ablation plume to yield ZnO must also be addressed. Since ZnO suppresses the formation of Cu oxides, the formation of the oxide, at least to an appreciable extent, is likely to take place within the liquid phase. Moreover, it is worth mentioning that the ultrasound treatment described in the experimental section only affected the non-irradiated region of the metal support where a ZIF-8 layer was weakly attached to the surface, as Figure 2a demonstrates. This implies that the laser ablation, without being the key factor to grow the MOF on the metal, was important to produce strong adhesion of the MOF crystals in the irradiated region. Finally, no crystalline phases other than ZIF-8 were observed by XRD (Figure 3).

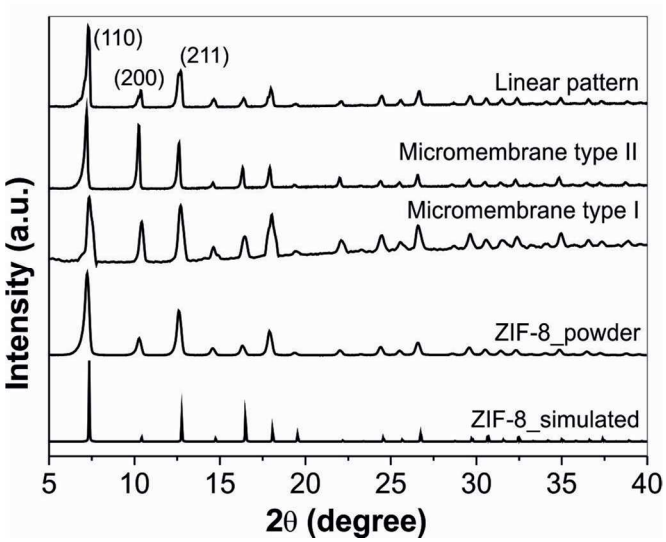

Figure 3. XRD patterns of the different samples obtained (smooth or outlet side in case of micromembranes) as compared to the powder and simulated diffractograms.

ZIF-8 micromembranes

The previous linear patterns inspired us to perforate brass supports by laser irradiation to induce porosity and subsequently crystallize ZIF-8 micromembranes. In this case (Figure 1c-1f), as the brass support was irradiated, molten material from inside the perforations was deposited around them, forming rougher edges on the side of the support where the laser beam was focused (rough or inlet side). In general, the outlet side of the support was less affected by the irradiation. As described in the experimental section, two laser irradiation conditions (types I and II, see Table 1) were used to drill microholes of various diameters, spaced at different distances and surrounded by distinct rough edges. The Rofin-Sinar laser used to perforate type I supports gave rise to large hole diameters (72 (±12) and 20 (±2) μm in the inlet and outlet sides of the laser, respectively) with elliptical shapes and very rough

edges (Figure 1c and 1d). In contrast, the EasyMark-20 laser used to generate type II supports, with a lower powder density than the Rofin-Sinar laser, had both better beam quality to control the pulse and longer pulse width needing fewer scans to perforate the surface. This led to smaller circular perforations (59 (±1) and 32 (±2) μm in the inlet and outlet sides of the laser, respectively), almost without rough edges (Figure 1e and 1f). Besides, the entrance and exit diameter dimensions with type II conditions were closer and had a narrower size distribution than with type I conditions. In agreement with our results, it has been reported that the power density strongly influences the mass ablation rate[48] and the crater morphology and diameter[49] upon laser irradiation.

The type I and type II conditions also provided a different number of holes per unit area, ca. 4400 and 22000 microholes·cm^{-2}, respectively, and a different degree of porosity, 1.6 (±0.2)% and 18 (±2)%, respectively, the control of which is important to maximize the membrane performance. In fact, there was a limitation on the maximum porosity that could be achieved because of the possibility of the support bending due to the high energy and temperature generated by the laser if the perforations are tightly spaced or a high number of scans is needed.

The same ZIF-8 solvothermal synthesis carried out on the previous linear pattern was applied to the perforated supports. Preferential heterogeneous nucleation and subsequent crystal growth of ZIF-8 around the rough edges of the perforations on both sides of the support was again promoted by the ZnO generated upon the laser irradiation. As shown in Figure 2, with both type I and type II supports, the smooth (outlet) side, having the smaller perforation diameter, was completely covered with ZIF-8 crystals (as identified by XRD in Figure 3), while the rough (inlet) side produced in every perforation a donut shape constituted by highly intergrown crystals. In any event, every hole was fully filled with crystalline material giving rise to a ZIF-8 micromembrane of a dimension corresponding to the smaller perforation diameter of the outlet side. This suggests that the micromembranes are suitable for testing by permeation analysis, after producing a macroscopic membrane composed of thousands of micromembranes (4400 and 22000 micromembranes·cm^{-2} for type I and type II samples, respectively) appropriate for permeation characterization. Finally, neither intensities coming from the brass substrate (first peak at 43.5º 2θ[29]) nor from the ZnO (masked by ZIF-8 coating) are appreciated in the XRD pattern shown in Figure 3.

Even if ZIF-8 has an isotropic pore structure unlike other porous systems such as the extensively studied MFI-type zeolite,[50,51] it may be of interest to calculate the degree of crystal orientation in the ZIF-8 membrane from the CPO (crystallographic preferred orientation) index. This has already been applied to ZIF-8 membranes prepared by seeding and secondary growth on porous alumina supports (where the CPO values were much higher than those obtained here)[52] using intensities corresponding to (200), (110) and (211) peaks:

$$CPO_{(200)/(110)} = \frac{\left(\frac{I_{(200)}}{I_{(110)}}\right)_S - \left(\frac{I_{(200)}}{I_{(110)}}\right)_P}{\left(\frac{I_{(200)}}{I_{(110)}}\right)_P}, \quad CPO_{(200)/(211)} = \frac{\left(\frac{I_{(200)}}{I_{(211)}}\right)_S - \left(\frac{I_{(200)}}{I_{(211)}}\right)_P}{\left(\frac{I_{(200)}}{I_{(211)}}\right)_P}$$

where I is the intensity of a given peak, and S and P refer to the sample (ZIF-8 coated brass support) and reference randomly oriented powder, respectively. The CPO is null when the intensity ratios in the sample and reference powder are the same. For a type I micromembrane (Figure 3), the $CPO_{(200)/(110)}$ and $CPO_{(200)/(211)}$ were 1.9 and 0.9, respectively, indicating some crystallographic preferential orientation of the {100} planes parallel to the metal sheet. The $CPO_{(200)/(110)}$ and $CPO_{(200)/(211)}$ were 2.9 and 2.7, respectively, for a type II micromembrane (Figure 3). Since the type I micromembranes (1.6% porosity) had a higher fraction of non-irradiated area than the type II micromembranes (18% porosity), these CPO values suggest that the growth on the brass surface tended to be more randomly oriented than that on the perforations. This analysis was made considering the ZIF-8 grown on the smooth (outlet) side of the laser perforated sheet. In fact, Figure S3 compares XRD patterns for ZIF-8 growing on both the rough (inlet) and smooth (outlet) sides of the sheet, the $CPO_{(200)/(110)}$ and $CPO_{(200)/(211)}$ values being 0.0 and 0.1, respectively, for the rough side, i.e. with no crystallographic preferential orientation.

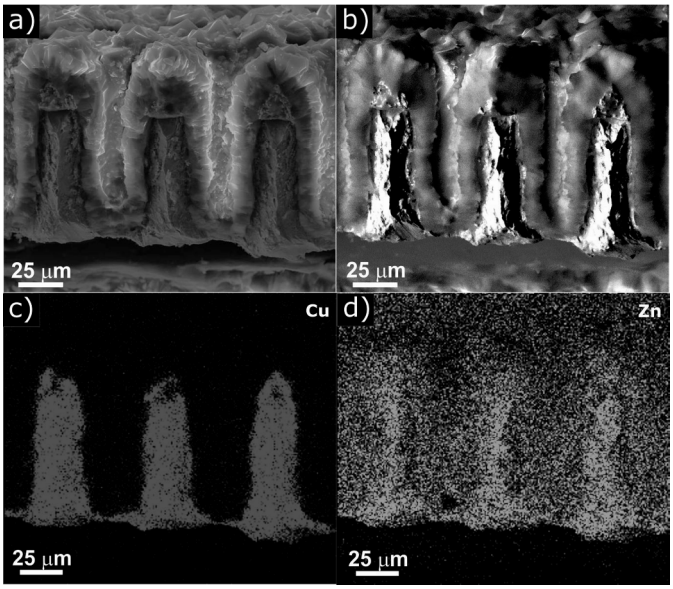

Figure 4. Cross section of a type II micromembrane: a) SEM image with top and bottom parts corresponding to inlet and outlet irradiation sides, respectively; b) backscattering SEM image; c-d) Cu and Zn, respectively, EDX mapping of the same previous images.

SEM and EDX analyses of a cross section of the type II micromembranes (Figure 4) revealed the presence of ZIF-8 crystals thoroughly filling the microperforations. In addition, crystals clearly nucleated on the laser-activated inner surface of every microperforation, as the columnar growth (Figure 4a and

4b) carpeting the internal surface of the microperforations suggests. This columnar growth observed on the rough or inlet side was not perceived as XRD orientation due to the fact that a significant part of the growing surface (the inner part of the microperforations) is perpendicular to the brass sheet surface scanned by the X-rays. The EDX mapping (Figures 4c and 4d) allows us to distinguish between the brass support (with green Cu not participating in the MOF composition) and the crystallized ZIF-8.

Performance of ZIF-8 micromembranes

Regardless of the type of micromembrane, the TGA analysis of ZIF-8 powder recovered after the micromembrane synthesis showed no weight loss related to either solvent or ligand trapped in the MOF micropores (Figure S4). In fact, the weight loss started at temperatures higher than about 400 °C which proved that the membrane preparation yielded guest-free, activated ZIF-8. After heating at 850 °C, the ZIF-8 framework decomposed and the solid residue obtained was ZnO.

The BET specific surface area values corresponding to type I and type II micromembranes obtained upon N_2 adsorption were 201 and 181 m^2/g, respectively. The amount of ZIF-8 in these two samples was 6.5 and 9.1 wt%, respectively; the greater the porosity of the irradiated support, the higher the yield of ZIF-8 per support mass unit. We infer from these adsorption parameters that the ZIF-8 material in the micromembranes is accessible for the gas transport. Thus the membranes were evaluated for the separation of H_2/CH_4, CO_2/CH_4, He/CH_4 and O_2/N_2 equimolar mixtures. The practical interest of these mixtures deals with hydrogen economy and methane upgrading[14,15] and the less studied He recovery.[53] Given the 3.4 Å ZIF-8 pore dimension and the fact that the kinetic diameters of the tested molecules He, H_2, CO_2, O_2, N_2 and CH_4 are 2.6, 2.9 and 3.3, 3.46, 3.64 and 3.8 Å, respectively, it is easy to predict molecular sieving effects for the above-mentioned gas pairs, even though the flexibility of the MOF has been claimed to justify the measurement of lower separation factors than expected.[31]

First, the performance of our samples is compared to ZIF-8 membranes on other previously reported kinds of supports (Table 2). The total membrane area evaluated was in the 0.6-1.0 cm^2 range, composed of thousands of micromembranes. Each micromembrane has a permeable area of a few hundreds of square micrometers (considering the outlet diameters in Table 1): 314 μm^2 (type I micromembrane) and 804 μm^2 (type II micromembrane). The permeance of the micromembrane arrays was calculated here by dividing the total permeation flux ($mol \cdot s^{-1} \cdot Pa^{-1}$) by the porous (microperforated) area. Our ZIF-8 micromembranes could be said to be self-supported, since both membrane sides (permeate and retentate) are in contact through the selective microporous material ZIF-8. In a traditional supported membrane, the support itself stands between the selective material and one of the membrane sides. This idea has already been put forward in our previous publication concerning zeolite silicalite-1;[44] it is worth mentioning that the present research with ZIF-8 has advantages over the study with silicalite-1. Brass is used instead of stainless steel and there is no need for seeding and activation processes. Nevertheless, a drawback of our micromembranes is the large thickness (at least that of the metallic sheet). Despite this limitation, the micromembrane H_2 permeances are among the highest reported in the literature (Table 2) with acceptable H_2/CH_4 selectivity values.

Figure 5 depicts the performance of the ZIF-8 micromembranes in separating the three mixtures mentioned above. In the case of the He/CH_4 mixture, the He permeance is lower than that of H_2 in the H_2/CH_4 mixture, and this translates into lower He/CH_4 selectivity. This may be due to possible transport through membrane defects where the Knudsen diffusion mechanism could be important favoring H_2 permeance, with lower molecular weight (2), over that of He (molecular weight 4). In any event, He permeated faster than CH_4, and selectivities of 4.1 (±0.3) and 8.7 (±0.6) were measured for type I and type II micromembranes with He permeances of 110 (±27)·10^{-8} and 8.0 (±0.0)·10^{-8} $mol \cdot m^{-2} \cdot s^{-1} \cdot Pa^{-1}$, respectively. These values mean that our micromembranes would be useful for recovering He from natural gas. Concerning the other mixture in Figure 5 (CO_2/CH_4), no really good results were achieved, in line with previous works where the low CO_2 adsorption of ZIF-8 is discussed.[56] A result even worse due to size similarities of the molecules was observed with the O_2/N_2 mixture where a type II micromembrane showed O_2/N_2 selectivity of 1.7 (with O_2 permeance of 1.2·10^{-10} $mol \cdot m^{-2} \cdot s^{-1} \cdot Pa^{-1}$) below the 2.0 and 2.5 ideal selectivity values reported by Bux et al.[31] and Shekhah et al.[42], respectively, for ZIF-8 membranes.

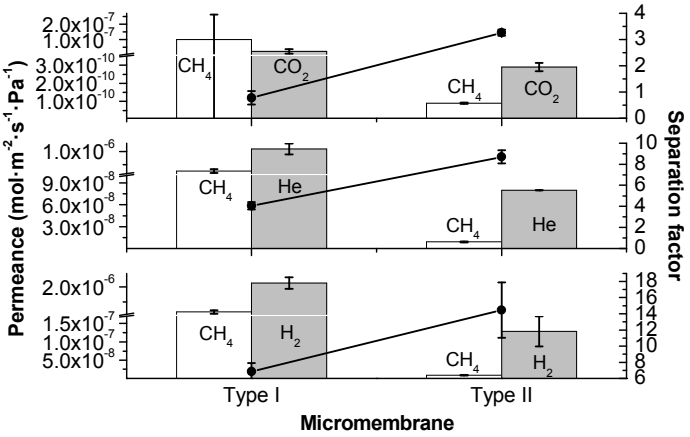

Figure 5. Permeances and separation factors obtained at 35 ºC corresponding to H_2/CH_4, He/CH_4 and CO_2/CH_4 mixtures as a function of micromembrane type.

The H_2/CH_4 separation performance was evaluated as a function of temperature (Figure 6) for the more permeable type I micromembrane. In the 35-150 ºC temperature range, H_2 and CH_4 permeances showed weak activation: the corresponding apparent activation energies were 4.0 and 4.3 $kJ \cdot mol^{-1}$, respectively. This energy difference favorable to CH_4 explains the observed decrease in H_2/CH_4 selectivity from 7.9 at 35 ºC to 5.5 at 150 ºC. On completion of the experiment during which the temperature was increased, the temperature was returned to

Table 2. Separation of the H_2/CH_4 mixture with ZIF-8 micromembranes as compared to the results in the literature.

Support	Thickness [μm]	Temperature [ºC]	H_2 permeance·10^8 [mol·m^{-2}·s^{-1}·Pa^{-1}]	Permeability [Barrer]	H_2/CH_4 selectivity	Reference
Al_2O_3 disc	12	25	10.0	3590	15.0	Bux et al.[52]
TiO_2 disc	30	25	5.0	4480	11.3	Bux et al.[31]
TiO_2 disc	30	20	13.3	11900	16.0	Hertäg et al.[54]
Al_2O_3 disc	20	25	17.3	10300	13.0[a]	McCarthy et al.[34]
Al_2O_3 disc	15	25	9.0	4040	15.0	Diestel et al.[37]
Al_2O_3 disc	0.5	35	1.9	26	9.5[a]	Shekhah et al.[42]
Al_2O_3–ZnO disc	8	25	20.8	4980	10.4	Zhang et al.[46]
SiO_2 wafer	95	25	32.8	93200	4.8	Fan et al.[40]
Al_2O_3 tube	2.5	22	139	10400	10.7	Pan et al.[39]
Al_2O_3 tube	2	25	40.0	2390	12.1	Huang et al.[55]
Perforated brass	75	35	226 ± 38	507000	6.9 ± 1.1	This work (type I)
Perforated brass	75	35	12.8 ± 4.1	28700	14.4 ± 3.4	This work (type II)

[a]Ideal selectivity

its initial value (35 ºC) and the membrane performance evaluated again, yielding H_2 and CH_4 permeances of $2.0\cdot10^{-6}$and $2.5\cdot10^{-7}$ mol·m^{-2}·s^{-1}·Pa^{-1}, respectively. These values are comparable to the corresponding initial values of $1.9\cdot10^{-6}$ and $2.4\cdot10^{-7}$ mol·m^{-2}·s^{-1}·Pa^{-1}, confirming the thermal stability of the ZIF-8 micromembrane. In any event, the high H_2/CH_4 and He/CH_4 separation selectivity values achieved corroborate the membrane continuity observed by the above characterization

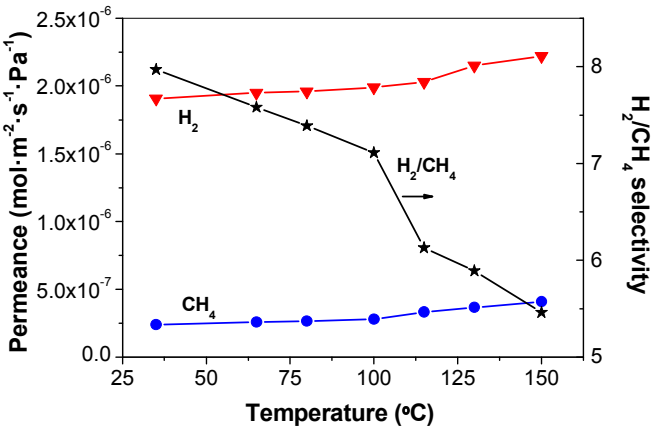

Figure 6. Separation of the H_2/CH_4 mixture as a function of temperature for a type I micromembrane.

From the point of view of separation performance, type I membranes with lower selectivities and higher permeabilities than type II membranes (Figure 5) must have in consequence a higher density of defects. However, there is no clear correlation between permeance and selectivity values in the case of the membranes in Table 2; this may be due to the different supports and synthesis conditions used. Finally, the errors in Table 2 and Figures 5 and 6 were produced by averaging the performance of three different membranes of each type prepared under the same conditions. This confirms the reliability of our membrane synthesis and characterization approach.

Conclusion

Nd-YAG laser techniques were used for the drilling of brass sheets leading to porous supports with 1.6 and 18% porosities and 20-32 μm effective microperforation diameters. The inherent properties of brass as a metal support together with its chemical compatibility with the MOF and the laser support activation (generation of roughness and ZnO from Zn oxidation) promoted the nucleation and crystal growth of ZIF-8 micromembranes. These micromembranes incorporated ZIF-8 not only on the support surface but also inside the holes of the support, as demonstrated by SEM observation. XRD characterization demonstrated both the preparation of pure ZIF-8 phase and the achievement of some degree of crystallographic preferential orientation of the {100} planes parallel to the metal sheet.

The N_2 adsorption experiments revealed full access of N_2 adsorbate to the ZIF-8 material in the micromembranes, corroborated by the measurement of permeances for several gas mixtures of interest. The reproducibly prepared ZIF-8 micromembranes were able to separate with high selectivity both H_2/CH_4 and He/CH_4 mixtures with respective separation factors of 14.4 (±3.4) and 8.7 (±0.6), far above the corresponding Knudsen values and among the best published to date. Regarding the CO_2/CH_4 and O_2/N_2 mixtures, no satisfactory separation was achieved. These results, together with the observation of temperature activated transport for the H_2/CH_4 mixture, allow us to infer that we have a high quality, continuous membrane with transport through the micropores (i.e. not through membrane defects).

Acknowledgements

Financial support (MAT2010-15870 and MAT2010-18519) and FPU Program fellowships (M. N. and B. S.) from the Spanish MINECO, the Aragón Government and the ESF are gratefully acknowledged. Authors would like to acknowledge the use of Servicio General de Apoyo a la Investigación-SAI (Universidad de Zaragoza).

Notes and references

a Chemical and Environmental Engineering Department and Nanoscience Institute of Aragón (INA), Universidad de Zaragoza, 50018 Zaragoza, Spain. *Fax:* +34 976 761879, *Tel:* +34 976 762471, *Email*:* coronas@unizar.es.
b Department of Earth Sciences, Universidad de Zaragoza, 50009 Zaragoza, Spain.
c Departamento de Didáctica de las Ciencias Experimentales, Universidad de Zaragoza, 50009 Zaragoza, Spain.
d Instituto de Ciencia de Materiales de Aragón, CSIC-Universidad de Zaragoza, 50018 Zaragoza, Spain
†Electronic Supplementary Information (ESI) available: [micromembrane image, XRD and TGA analyses]. See DOI: 10.1039/b000000x/

1 G. Ferey, *Chem. Soc. Rev.,* 2008, **37**, 191-214.
2 D. J. Tranchemontagne, J. L. Mendoza-Cortes, M. O'Keeffe and O. M. Yaghi, *Chem. Soc. Rev.,* 2009, **38**, 1257-1283.
3 H. K. Chae, D. Y. Siberio-Perez, J. Kim, Y. Go, M. Eddaoudi, A. J. Matzger, M. O'Keeffe and O. M. Yaghi, *Nature,* 2004, **427**, 523-527.
4 G. Ferey, C. Serre, *Chem. Soc. Rev.,* 2009, **38**, 1380-1399.
5 M. Eddaoudi, J. Kim, N. Rosi, D. Vodak, J. Wachter, M. O'Keeffe and O. M. Yaghi, *Science,* 2002, **295**, 469-472.
6 Z. Wang and S. M. Cohen, Chem. *Soc. Rev.*, 2009, **38**, 1315-1329.
7 H. Furukawa, N. Ko, Y. B. Go, Aratani, N.; S. B. Choi, E. Choi, A. O. Yazaydin, R. Q. Snurr, M. O'Keeffe, J. Kim and O. M. Yaghi, *Science,* 2010, **329**, 424-428.
8 N. Liedana, A. Galve, C. Rubio, C. Tellez and J. Coronas, ACS Appl. *Mater. Interfaces,* 2012, **4**, 5016-5021.
9 P. Horcajada, T. Chalati, C. Serre, B. Gillet, C. Sebrie, T. Baati, J. F. Eubank, D. Heurtaux, P. Clayette, C. Kreuz, J. S. Chang, Y. K. Hwang, V. Marsaud, P. N. Bories, L. Cynober, S. Gil, G. Ferey, P. Couvreur and R. Gref, *Nat. Mater.,* 2010, **9**, 172-178.
10 V. Finsy, H. Verelst, L. Alaerts, D. De Vos, P. A. Jacobs, G. V. Baron and J. F. M. Denayer, *J. Am. Chem. Soc.,* 2008, **130**, 7110-7118.
11 S. Couck, J. F. M. Denayer, G. V. Baron, T. Rémy, J. Gascon and F. Kapteijn, *J. Am. Chem. Soc.,* 2009, **131**, 6326-6327.
12 J. M. Zamaro, N. C. Perez, E. E. Miro, C. Casado, B. Seoane, C. Tellez and J. Coronas, *Chem. Eng. J.,* 2012, **195**, 180-187.
13 G. Lu, O. K. Farha, W. Zhang, F. Huo and J. T. Hupp, *Adv. Mater.,* 2012, **24**, 3970-3974.
14 J. Gascon, F. Kapteijn, B. Zornoza, V. Sebastian, C. Casado and J. Coronas, *Chem. Mater.,* 2012, **24**, 2829-2844.
15 P. Bernardo, E. Drioli and G. Golemme, *Ind. Eng. Chem. Res.,* 2009, **48**, 4638-4663.
16 J. Caro and M. Noack, *Microporous Mesoporous Mater.,* 2008, **115**, 215-233.
17 O. Shekhah, J. Liu, R. A. Fischer and C. Woll, *Chem. Soc. Rev.,* 2011, **40**, 1081-1106.
18 Y. Morigami, M. Kondo, J. Abe, H. Kita and K. Okamoto, *Sep. Purif. Technol.,* 2001, **25**, 251-260.
19 J. Coronas and J. Santamaria, *Chem. Eng. Sci.,* 2004, **59**, 4879-4885.
20 P. Falcaro, D. Buso, A. J. Hill and C. M. Doherty, *Adv. Mater.,* 2012, **24**, 3153-3168.
21 P. Falcaro, A. J. Hill, K. M. Nairn, J. Jasieniak, J. I. Mardel, T. J. Bastow, S. C. Mayo, M. Gimona, D. Gomez, H. J. Whitfield, R. Ricco, A. Patelli, B. Marmiroli, H. Amenitsch, T. Colson, L. Villanova and D. Buso, *Nat. Commun.,* 2011, **2**, 237-244.
22 R. Ricco, L. Malfatti, M. Takahashi, A. J. Hill and P. Falcaro, *J. Mater. Chem. A,* 2013, **1**, 13033-13045.
23 Y. Yoo and H.-K. Jeong, *Chem. Commun.,* 2008, 2441-2443.
24 R. Ameloot, E. Gobechiya, H. Uji-i, J. A. Martens, J. Hofkens, L. Alaerts, B. F. Sels and D. E. De Vos, *Adv. Mater.,* 2010, **22**, 2685-2688.
25 D. Witters, S. Vermeir, R. Puers, B. F. Sels, D. E. De Vos, J. Lammertyn and R. Ameloot, *Chem. Mater.,* 2013, **25**, 1021-1023.
26 R. Ameloot, L. Pandey, M. V. der Auweraer, L. Alaerts, B. F. Sels and D. E. De Vos, *Chem. Commun.,* 2010, **46**, 3735-3737.
27 C. Dimitrakakis, C. D. Easton, B. W. Muir, B. P. Ladewig and M. R. Hill, *Cryst. Growth Des.,* 2013, **13**, 4411-4417.
28 C. Dimitrakakis, B. Marmiroli, H. Amenitsch, L. Malfatti, P. Innocenzi, G. Grenci, L. Vaccari, A. J. Hill, B. P. Ladewig, M. R. Hill and P. Falcaro, *Chem. Commun.,* 2012, **48**, 7483-7485.
29 C. G. Park, J. G. Kim, Y. M. Chung, J. G. Han, S. H. Ahn and C. H. Lee, *Surf. Coat. Technol.,* 2005, **200**, 77-82.
30 K. S. Park, Z. Ni, A. P. Cote, J. Y. Choi, R. D. Huang, F. J. Uribe-Romo, H. K. Chae, M. O'Keeffe and O. M. Yaghi, *Proc. Natl. Acad. Sci. U. S. A.,* 2006, **103**, 10186-10191.
31 H. Bux, F. Y. Liang, Y. S. Li, J. Cravillon, M. Wiebcke and J. Caro, *J. Am. Chem. Soc.,* 2009, **131**, 16000-16001.
32 S. R. Venna and M. A. Carreon, *J. Am. Chem. Soc.,* 2010, **132**, 76-78.
33 Y. Pan, B. Wang and Z. Lai, *J. Membr. Sci.,* 2012, **421-422**, 292-298.
34 M. C. McCarthy, V. Varela-Guerrero, G. V. Barnett and H.-K. Jeong, *Langmuir*, 2010, **26**, 14636-14641.
35 D. Fairen-Jimenez, S. A. Moggach, M. T. Wharmby, P. A. Wright, S. Parsons and T. Duren, *J. Am. Chem. Soc.,* 2011, **133**, 8900-8902.
36 Y. Pan, T. Li, G. Lestari, Z. Lai, *J. Membr. Sci.,* 2012, **390–391**, 93-98.
37 L. Diestel, H. Bux, D. Wachsmuth and J. Caro, *Microporous Mesoporous Mater.,* 2012, **164**, 288-293.
38 M. J. C. Ordonez, K. J. Balkus, J. P. Ferraris and I. H. Musselman, *J. Membr. Sci*., 2010, **361**, 28-37.
39 Y. C. Pan, B. Wang and Z. P. Lai, *J. Membr. Sci.,* 2012, **421**, 292-298.
40 L. L. Fan, M. Xue, Z. X. Kang, H. Li and S. L. Qiu, *J. Mater. Chem.,* 2012, **22**, 25272-25276.
41 Y. C. Pan and Z. O. Lai, *Chem. Commun.,* 2011, **47**, 10275-10277.
42 O. Shekhah, R. Swaidan, Y. Belmabkhout, M. du Plessis, T. Jacobs, L. J. Barbour, I. Pinnau, M. Eddaoudi, *Chem. Commun.,* 2014, **50**, 2089-2092.
43 L. Dumee, L. He, M. Hill, B. Zhu, M. Duke, J. Schutz, F. S. She, H. T. Wang, S. Gray, P. Hodgson and L. X. Kong, *J. Mater. Chem. A,* 2013, **1**, 9208-9214.
44 E. Mateo, R. Lahoz, G. F. de la Fuente, A. Paniagua, J. Coronas and J. Santamaria, *Chem. Mater.,* 2004, **16**, 4847-4850.
45 M. Shah, H. T. Kwon, V. Tran, S. Sachdeva and H. K. Jeong, *Microporous Mesoporous Mater.,* 2013, **165**, 63-69.
46 X. F. Zhang, Y. G. Liu, L. Y. Kong, H. O. Liu, J. S. Qiu, W. Han, L. T. Weng, K. L. Yeung and W. D. Zhu, *J. Mater. Chem. A,* 2013, **1**, 10635-10638.
47 D. N. Patel, P. K. Pandey and R. K. Thareja, *Appl. Opt.,* 2013, **52**, 7592-7601.

48 R. E. Russo, X. L. Mao, M. Caetano, M. A. Shannon, *Appl. Surf. Sci*., 1996, **96-98**, 144-148.
49 D. N. Patel, R. P. Singh and R. K. Thareja, *Appl. Surf. Sci.,* 2014, **288**, 550-557.
50 Z. P. Lai, G. Bonilla, I. Diaz, J. G. Nery, K. Sujaoti, M. A. Amat, E. Kokkoli, O. Terasaki, R. W. Thompson, M. Tsapatsis and D. G. Vlachos, *Science,* 2003, **300**, 456-460.
51 E. Mateo, R. Lahoz, G. F. de la Fuente, A. Paniagua, J. Coronas and J. Santamaria, *Chem. Mater.,* 2007, **19**, 594-599.
52 H. Bux, A. Feldhoff, J. Cravillon, M. Wiebcke, Y.-S. Li and J. Caro, *Chem. Mater.,* 2011, **23**, 2262-2269.
53 F. Cao, C. Zhang, Y. Xiao, H. Huang, W. Zhang, D. Liu, C. Zhong, Q. Yang, Z. Yang, X. Lu, *Ind. Eng. Chem. Res.,* 2012, **51**, 11274-11278.
54 L. Hertäg, H. Bux, J. Caro, C. Chmelik, T. Remsungnen, M. Knauth and S. Fritzsche, *J. Membr. Sci.,* 2011, **377**, 36-41.
55 K. Huang, Z. Dong, Q. Li and W. Jin, *Chem. Commun.,* 2013, **49**, 10326-10328.
56 B. Zornoza, B. Seoane, J. M. Zamaro, C. Tellez and J. Coronas, *ChemPhysChem,* 2011, **12**, 2781-2785.

Graphical abstract and contents text

ZIF-8 micromembranes for gas separation prepared on laser-perforated brass supports

Marta Navarro, Beatriz Seoane, Ester Mateo, Ruth Lahoz, Germán F. de la Fuente and Joaquín Coronas*

MOF micromembranes of 20-32 μm in diameter were prepared by synthesizing ZIF-8 on Nd-YAG laser-perforated 75 μm thick brass sheets (63/37 Cu/Zn). The membranes were applied to the separation of H_2/CH_4, He/CH_4 and CO_2/CH_4 mixtures.